Solution Structure of Eps15's Third EH Domain Reveals Coincident Phe−Trp and Asn−Pro−Phe Binding Sites[†,‡]

Jennifer L. Enmon,[§] Tonny de Beer,[||] and Michael Overduin*[,||]

Department of Chemistry and Biochemistry, University of Colorado, Boulder, Colorado 80309, and Department of Pharmacology, University of Colorado Health Sciences Center, 4200 East Ninth Avenue, Denver, Colorado 80262

Received November 29, 1999; Revised Manuscript Received February 9, 2000

ABSTRACT: Eps15 homology (EH) domains interact with proteins involved in endocytosis and signal transduction. EH domains bind to Asn−Pro−Phe (NPF) consensus motifs of target proteins. A few EH domains, such as the third EH domain (EH_3) of human Eps15, prefer to bind Phe−Trp (FW) sequences. The structure of EH_3 has been solved by nuclear magnetic resonance (NMR) spectroscopy and is the first of an FW- and NPF-binding EH domain. Both FW and NPF sequences bind in the same hydrophobic pocket as shown by heteronuclear chemical shift mapping. EH_3 contains the dual EF-hand fold characteristic of the EH domain family, but it binds calcium with high affinity in the first EF-hand rather than the usual coordination in the second EF-hand. Point mutations were designed based on differences in the EH_3 and the second EH domain (EH_2) of human Eps15 that alter the affinity of the domains for FW or NPF motif peptides. Peptides that mimic binding sites in the potential EH_3 targets Rab, synaptojanin, and the cation-dependent mannose 6-phosphate receptor were used to explore wild-type and mutant affinities. Characterization of the structure and binding properties of an FW- and NPF-binding EH domain and comparison to an NPF-specific EH domain provide important insights into the mechanisms of EH domain ligand recognition.

The Eps15 homology (EH)[1] domain is a eukaryotic signaling module that mediates the formation of macromolecular complexes by binding short protein sequences (reviewed in ref *1*). Like src homology 3 (SH3) domains, EH domains bind specifically but with moderate affinity to short, unmodified motifs through predominantly hydrophobic interactions (*2*, *3*). The target motifs are divided into three classes: class I consists of the consensus Asn−Pro−Phe (NPF) sequence; class II consists of aromatic and hydrophobic di- and tripeptide motifs, including the Phe−Trp (FW), Trp−Trp, and Ser−Trp−Gly motifs; and class III contains the His−(Thr/Ser)−Phe motif (*3*). Multiple putative NPF-binding sequences have been identified in EH domain interacting proteins such as AP180 (*4*), Rab (Hrb) (*2*), Numb (*2*), synaptojanin (*5*), and epsin (*6*). An FW sequence has been implicated as a sorting motif for the cation-dependent mannose 6-phosphate receptor (MPR) (*7*, *8*).

A double EF-hand fold is predicted to be shared throughout the EH domain family based on the structure of a prototypic member, EH_2, and on structure-based sequence alignment (*9*). In addition, EH domains are generally found in tandem series of two to three repeats (*10*), and they are often juxtaposed with coiled coil regions that mediate protein oligomerization (*11*). Therefore, multivalent EH domain interactions may amplify the strength and the specificity of the interactions. Alternatively, weak, monovalent EH domain interactions may facilitate transient interactions between proteins in dynamic signaling and endocytic pathways. The structural basis of such interactions is important for understanding how a growing number of EH domain proteins including Eps15R (*12*), intersectin (*13*), γ-synergin (*14*), and EHD1 (*15*) are recruited to the endocytic machinery.

Eps15 consists of several recognition sites and binding domains that interact with other components of the endocytic machinery. Eps15 was originally identified as a substrate of the human epidermal growth factor receptor and is composed of three regions (*12*). The C-terminal region is bound by α-adaptin of the adaptor protein-2 complex (*16*−*19*), and the three EH domains in Eps15's N-terminus are thought to recruit proteins to this complex during clathrin-dependent endocytosis. Eps15's central coiled coil domain mediates formation of homodimers (*11*) as well as heterodimers with other EH domain proteins such as intersectin (*20*) and Eps15R (*21*). This oligomerization could serve to recruit a wide array of endocytic proteins to the rim of clathrin-coated pits.

[†] Grant support was provided by the National Institutes of Health (CA 77585) and the Pew Scholar's Program (M.O.). The NMR Center is supported by the Howard Hughes Medical Institute. T.d.B. is the recipient of a National Institutes of Health Fellowship Award (CA 74466).

[‡] The structure was deposited in the Protein Data Bank under Accession No. 1C07.

* To whom correspondence should be addressed. E-mail: Michael.Overduin@UCHSC.edu. Fax: (303) 315-7097. Phone: (303) 315-8774.

[§] University of Colorado at Boulder.

[||] University of Colorado Health Sciences Center.

[1] Abbreviations: DTT-*d*, perdeuterated dithiothreitol; EDTA, ethylenediaminetetraacetic acid; EH, Eps15 homology; EH_3, third EH domain of human Eps15; EH_2, second EH domain of human Eps15; mEH_1, first EH domain of mouse Eps15; FW, Phe−Trp; FW_{PDL}, DSTPGQVAFW; FW_{MPR}, DMEQFPHLAFWQDL; NPF, Asn−Pro−Phe; NPF_{RAB}, PTGSSSTNPFL; NPF_{SYN}, RTAAPGNPFRVQ; MPR, cation-dependent mannose 6-phosphate receptor; NMR, nuclear magnetic resonance; NOE, nuclear Overhauser effect; rmsd, root mean square deviation; RU, response unit.

10.1021/bi9927383 CCC: $19.00
Published on Web 03/23/2000

The structures of two of Eps15's three EH domains have been determined (*9*, *22*). However, the most functionally divergent of its three EH domains, EH_3, has yet to be characterized in detail. EH_3 primarily selects for Phe−Trp (FW) sequences from peptide phage-displayed libraries, while the first two EH domains of Eps15, like most EH domains, select for peptides containing NPF (*3*). Although NPF has not been eliminated as a binding target recognized by EH_3, its affinity for most NPF sequences has been reported as negligible (*3*). An NPF-binding pocket has been identified in EH_2 (*9*) and in the first EH domain of mouse Eps15 (mEH_1) (*22*). However, the precise location of the binding pocket for FW has not yet been defined.

EH_3 has a canonical calcium-binding sequence (*23*) in its first EF-hand in contrast to most identified EH domains, which contain canonical calcium-binding sequences in the second EF-hand. Indeed, it has been demonstrated that EH_2 binds calcium in only the second helix−loop−helix (*9*). Other members of the EF-hand superfamily, such as calmodulin (*24*) and troponin C (*25*), exhibit dramatic structural changes depending upon calcium occupancy, yet calcium occupancy has little effect on the structure of calbindin D9k (*26*). Therefore, the effect of the unusual location of EH_3's calcium-binding site on its overall structure cannot be predicted. Furthermore, considering the proximity of the calcium-binding site to the conserved NPF-binding pocket (*9*), the position of the calcium-binding site could contribute to EH_3's specificity.

To elucidate the FW-, NPF-, and calcium-binding properties of EH_3, the structure has been solved by multidimensional heteronuclear magnetic resonance (NMR) spectroscopy, and interactions with peptides representative of possible EH_3 ligand sites in Rab, synaptojanin, and MPR were characterized by NMR, surface plasmon resonance, and site-directed mutagenesis.

MATERIALS AND METHODS

Cloning of EH_3 and Mutagenesis of EH_3 and EH_2. A DNA fragment encoding amino acids 214−317 of human Eps15, which corresponds to its third EH domain, was obtained by PCR using full-length Eps15 cDNA as a template and was cloned into the *Bam*H1 and *Kpn*1 sites of the pRSETA vector (Invitrogen), which encodes for an N-terminal histidine tag followed by an enterokinase cleavage site. All mutants of EH_3 and EH_2 were created by site-directed mutagenesis (Quick Change, Stratagene). To prevent EH_3 dimerization (see NMR sample preparation), the EH_3(C274S) construct was used to produce all EH_3 mutants. All sequences were confirmed by dideoxysequencing.

NMR Sample Preparation. *Escherichia coli* strain B834 pLys S was transformed with pRSET-EH domain constructs and grown in either Luria broth or, for ^{15}N-labeled samples, in M9 minimal media supplemented with $^{15}NH_4Cl$ (1 g L^{-1}) (all isotope-labeled compounds from Cambridge Isotope Laboratories), glucose (3 g L^{-1}), ^{15}N-L-methionine (40 μg mL^{-1}), $CaCl_2$ (0.1 mM), $MgSO_4$ (2 mM), and vitamin solution (5 mL L^{-1}) (Centrum). For uniformly $^{15}N/^{13}C$-labeled samples, the M9 minimal media was enriched with ^{13}C-glucose (1.5 g L^{-1}), $^{15}NH_4Cl$ (1 g L^{-1}), and $^{15}N/^{13}C$-L-methionine (40 μg mL^{-1}). Cells were collected 3−5 h after induction with isopropyl-1-thio-β-D-galactopyranosidase (0.5 mM). Bacteria were lysed by freeze−thaw in lysis buffer [20 mM Tris, 100 mM KCl, 0.5 mM phenylmethanesulfonyl fluoride, 10 μg mL^{-1} leupeptin, 5 μg mL^{-1} antipain, 10 μg mL^{-1} soybean trypsin inhibitor, 2 mM NaN_3, 1 mM benzamidine, 10 μg mL^{-1} 1-chloro-3-tosylamido-7-amino-L-2-heptanone, 0.2% (v/v) Triton X-100, 0.2% (v/v) NP-40, and 0.2% (v/v) Tween-20, pH 8.0]. Cells were disrupted by sonication, and the His_6-tagged fusion protein was immobilized on Talon resin (Clontech) and eluted by cleavage with enterokinase (Invitrogen). The protease was removed with EK-Away beads (Invitrogen). Purified proteins were concentrated in 5-kDa limit concentrators (Millipore) and exchanged into NMR buffer [20 mM perdeuterated Tris, 100 mM KCl, 2 mM NaN_3, 2 mM $CaCl_2$, 10 μM 4-amidinophenylmethane sulfonyl fluoride, 100 μM−10 mM perdeuterated dithiothreitol (DTT-*d*), and 10 or 99.996% $^2H_2O/H_2O$, pH 6.5−7.8]. At millimolar concentrations, wild-type EH_3 forms disulfide-linked dimers through C^{274}. The repeated addition of 10 mM DTT-*d* and incubation at 37 °C for 1 h eliminated the dimer formation as determined by diffusion coefficients measured with pulsed field gradient NMR experiments (*27*). The formation of this disulfide bond has not been found to be relevant in Eps15 dimerization (*11*). Dimerization was prevented by site-directed mutagenesis of C^{274} to a serine (Quick Change, Stratagene). The structure is not perturbed by the mutation since the nuclear Overhauser effect (NOE) patterns exhibited in the ^{15}N-edited 3D NOESY spectra of wild-type EH_3 and EH_3(C274S) are virtually identical.

Data Collection and Assignment. All experiments were collected at 25 °C on Varian INOVA 500- and 600-MHz spectrometers equipped with triple resonance shielded probes. Spectra were processed with the NMRPipe package (*28*) and analyzed with PIPP (*29*) and in-house written software on Sun Microsystems and Silicon Graphics workstations (http://biomol.uchsc.edu). Assignments for backbone and side-chain resonances have been reported (*30*) and were primarily obtained from the HCC-TOCSY, CCC-TOCSY (*31*), HCCH-TOCSY (*32*), CBCA(CO)NH, HNCACB, and HNCO (*33*) experiments. Aromatic side chain residues were assigned using 2D spectra correlating Cβs with Hδs or Hϵs (*34*).

Angular and Distance Constraints. The ϕ and ψ angle restraints were obtained from a combination of the HNHA (*35*) and HMQC-J (*36*) experiments and $^1H\alpha$, $^{13}C\alpha$, and $^{13}C'$ chemical shifts (*37*). Interproton distance restraints were derived from cross-peak intensities in the 3D ^{15}N-NOESY, 3D and 4D ^{13}C-NOESY (*38*−*40*), and simultaneous 3D $^{15}N/^{13}C$-NOESY (*41*) experiments. Distance restraints were assigned upper bounds of 2.7 Å (strong), 3.5 Å (medium), and 5 Å (weak) and lower bounds of 0 Å based on the corresponding NOE cross-peak intensities and pseudo-atom corrections as recommended by Fletcher et al. (*42*).

Structure Generation and Statistical Analysis. The final structure calculation included 1613 distance restraints (671 intraresidue, 281 sequential, 338 medium range, and 323 long range), 45 φ angle restraints, 37 ψ angle restraints, and 24 pairs of hydrogen bond restraints. Also, six distance restraints between calcium and coordinating oxygen atoms were included in the final calculation based on average distances in high-resolution crystal structures of EF-hand proteins (*25*, *43*−*45*). Their inclusion did not perturb the structure of the protein backbone. Fifty structures were calculated by r^{-6} summation in a restrained molecular dynamics simulated

annealing protocol within the X-PLOR 3.84 software package (*46*). The 20 structures with the lowest NOE energies were analyzed with Procheck NMR (*47*). The coordinates of the ensemble of 20 NMR structures have been deposited under Accession No. 1C07 in the Protein Data Bank.

Calcium Titration. Mg^{2+}-bound EH_3(C274S) was prepared by precipitation of EH_3 by addition of 50−100 mM ethylenediaminetetraacetic acid (EDTA) (pH 8). The suspension was incubated at 37 °C for at least 1 h. The precipitate was then washed with 100 mM EDTA in 20 mM Tris and 100 mM KCl (pH 7.4) and incubated for an additional hour at 37 °C. The precipitate was dissolved in 7 M guanidinium hydrochloride, 20 mM Tris, and 100 mM KCl (pH 7.0) followed by slow dilution to a concentration of less than 0.2 M guanidinium hydrochloride with 20 mM Tris, 50 mM KCl, and 160 mM $MgCl_2$ (pH 7.4). The sample was then concentrated and exchanged into NMR buffer containing 160 mM $MgCl_2$ (pH 7.0). ^{15}N-Edited 3D NOESY (*38*) and 3D ^{15}N HSQC−NOESY−HSQC (*48*) spectra were collected for the Mg^{2+}-bound EH_3(C274S). Subsequently, calcium was titrated back into the NMR sample by the addition of aliquots of $CaCl_2$ in the $MgCl_2$-containing NMR buffer. ^{15}N/^{1}H HSQC (*49*, *50*) spectra were collected at 0, 0.07, 0.19, 0.37, 0.55, 0.74, 1.5, 2.2, 3.0, 3.7, 4.4, and 5.2 equiv of Ca^{2+}.

NPF Titration. Uniformly ^{13}C/^{15}N-labeled EH_3 (0.23 mM) in NMR buffer containing 21 mM DTT-*d* (pH 6.5) was titrated with an N-terminal biotinylated RTAAPGNPFRVQ peptide (NPF_{SYN}). (All peptides were obtained from Research Genetics.) Peptide was added from a 20 mM peptide stock in 98% $^2H_2O/H_2O$, and the pH of the sample was adjusted if necessary. ^{1}H/^{13}C HSQC and ^{1}H/^{15}N HSQC (*49*, *50*) experiments were collected at peptide concentrations of 0, 0.1, 0.5, 1.0, 1.5, and 2.0 mM.

FW Titration. Uniformly ^{15}N-labeled EH_3(C274S) (0.25 mM) in NMR buffer (pH 6.5) was titrated with increasing concentrations of DSTPGQVAFW peptide (FW_{PDL}). The peptide was added from 2.6 and 5.9 mM stocks in NMR buffer (pH 6.5). ^{1}H/^{15}N HSQC (*49*, *50*) experiments were collected before and after each addition. Uniformly labeled ^{15}N/^{13}C EH_3 (0.25 mM) in NMR buffer (pH 6.5) was lyophilized and redissolved in 99.996% $^2H_2O/H_2O$. This sample was titrated with FW_{PDL} peptide from a 4.75 mM stock in 99.996% $^2H_2O/H_2O$. The final concentration of FW_{PDL} was reached by addition of 0.5 mg of FW_{PDL}. The pH was adjusted with 1 M NaO^2H or 1 M ^2HCl. A set of ^{1}H/^{13}C HSQC (*49*, *50*) spectra were collected for both titrations at peptide concentrations of 0.01, 0.03, 0.10, 0.30, 0.58, and 1.23 mM. Uniformly ^{15}N-labeled EH_3(C274S) (1 mM) in NMR buffer (pH 7.0) was titrated with increasing concentrations of an N-terminal biotinylated DMEQFPHLAFWQDL peptide (FW_{MPR}). Peptide was added from 5.75 mM stock in NMR buffer at pH 7.0. ^{1}H/^{15}N HSQC (*49*, *50*) experiments were collected at 0.25, 0.50, 0.75, 1.0, 2.0, and 4.0 mM concentrations of FW_{MPR} peptide.

BIAcore Analysis. Protein samples were prepared as above and exchanged into BIAcore buffer [20 mM PIPES, 100 mM KCl, 100 μM DTT, 10 μM 4-amidinophenylmethane sulfonyl fluoride, 0.005% (v/v) Tween-20, 1 mM NaN_3, and 2 mM $CaCl_2$, pH 7.2]. Magnesium-bound EH_3 was prepared as above and exchanged into buffer that contained 160 mM $MgCl_2$ instead of 2 mM $CaCl_2$. The Mg^{2+} buffer was also used for the BIAcore experiments with this sample. Approximately 225 response units (RU) of an N-terminal biotinylated PTGSSSTNPFL peptide (NPF_{RAB}) and 176 RUs of an N-terminal biotinylated DSTPGQVAFW peptide (FW_{PDL}) were each bound to one cell of a streptavidin-coated sensor chip in a BIAcore 2000 instrument. A control cell was kept peptide-free for baseline corrections. Concentrations of protein ranging from 1 μM to 2 mM were injected with a flow rate of 30 μL min^{-1} in BIAcore buffer. Equilibrium RU values were estimated at each EH domain concentration by averaging the steady-state response after injection and correcting for the sample refractive index component (BIAevaluation 2.1).

RESULTS AND DISCUSSION

Structure Description. The solution structure of EH_3 was solved by a combination of three- and four-dimensional NMR experiments on ^{15}N- and ^{15}N/^{13}C-labeled protein. Fifty structures were calculated from 1613 distance, 24 hydrogen bond, 82 angle, and 6 calcium constraints using a simulated annealing protocol (Table 1). The superposition of the 20 structures with the lowest NOE violation energies is shown in Figure 1A and reveals four α-helices folded into a pair of EF-hands (Figure 1B). Helices αA, αB, αC, and αD span residues Ala^{223}−Thr^{235}, Gly^{245}−Leu^{253}, Ser^{259}−Cys^{269}, and Lys^{279}−Leu^{293}, respectively. The secondary structure elements are well-defined with a root mean square deviation (rmsd) for backbone atoms of 0.33 Å with respect to the average structure. The loops are also structurally well-defined, yielding an overall rmsd for backbone atoms of 0.45 Å for residues 218−309.

The structure of EH_3 consists of two helix−loop−helix motifs characteristic of EF-hand domains. The two EF-hand loops of EH_3 are associated through main chain hydrogen bonds and side chain packing interactions between residues Val^{243} and Leu^{277} in a β-sheet arrangement. The N-terminal αA helix is oriented approximately perpendicular to the other helices. The C-terminal αD helix is positioned roughly parallel to helix αB and is packed amid helices αA, αB, and αC. The αB helix has a kink between the first and the second turns and forms a V shape with the αC helix with an interhelical angle of ∼125° (Table 1). The C-terminal proline-rich region is an integral part of the EH_3 domain as evidenced by its packing against αD. The structural importance of the C-terminal region is supported by the loss of NPF-binding activity of EH domains in which the C-terminal region and a portion of αD is deleted (*3*).

Identification of the FW- and NPF-Binding Pocket. To identify the amino acid residues of EH_3 that are involved in FW and NPF binding, the interactions of EH_3 with FW- and NPF-containing peptides were studied by NMR. The peptides NPF_{RAB} (PTGSSSTNPFL) and NPF_{SYN} (RTAAPGNPFRVQ) match putative binding sequences in the Eps15-interacting proteins Rab (*2*) and synaptojanin (*5*), respectively. The two FW peptides, FW_{PDL} (DSTPGQVAFW) and FW_{MPR} (DMEQFPHLAFWQDL), were chosen based on EH_3's in vitro peptide selectivity from phage-displayed library screens (*3*) and on a protein sorting motif identified in the MPR (*7*), respectively.

The FW-binding pocket of EH_3 was located by ^{1}H, ^{13}C, and ^{15}N chemical shift mapping using a series of ^{1}H/^{15}N and ^{1}H/^{13}C heteronuclear single quantum coherence (HSQC)

Table 1: Statistics for EH_3 Structure[a]

Structure Generation			
NOEs[b]		torsional restraints	
intraresidue	671	φ	45
sequential	281	ψ	37
medium range	338	hydrogen bond	24
long range	323	calcium	6

Ramachandran Analysis[c]			
most favored regions	78.6%	generously allowed region	1.1%
additional allowed regions	19.4%	disallowed regions	0.8%

Average Energies (kcal mol^{-1})					
E_{total}	278 ± 16	$E_{dihedral}$	0.32 ± 0.14	E_{noe}	48.1 ± 6.6

Restraint Violations			
average NOE violations/structure >0.2 Å	3.1 ± 1.3	average angle violations/structure >2°	0.35 ± 0.49

Rmsd from Idealized Geometry					
bonds (Å)	0.0024 ± 0.00001	angles (deg)	0.58 ± 0.017	impropers (deg)	0.44 ± 0.001

Atomic Rmsd (Å)[d]

	backbone	all heavy atoms[e]		backbone	all heavy atoms[e]
secondary structure elements[f]	0.33 ± 0.07	0.73 ± 0.06	residues 218−309	0.45 ± 0.03	0.82 ± 0.07

Difference (Δ) in Interhelical Angles and Distances in EH_3 and Eps15 EH_2[g]

	angle (deg)			distance (Å)		
	EH_3	EH_2	Δ	EH_3	EH_2	Δ
αA and αB	130.1 ± 2.1	119.0 ± 2.4	11.1	13.68 ± 0.15	14.01 ± 0.23	0.42
αA and αC	102.8 ± 2.3	110.9 ± 2.1	8.1	17.40 ± 0.15	17.33 ± 0.18	0.07
αA and αD	118.4 ± 1.9	106.6 ± 2.0	11.8	9.48 ± 0.28	9.14 ± 0.16	0.34
αB and αC	125.6 ± 2.1	129.1 ± 2.2	3.5	11.21 ± 0.22	10.65 ± 0.15	0.56
αB and αD	16.16 ± 2.0	16.0 ± 2.1	0.1	11.49 ± 0.21	10.90 ± 0.14	0.59
αC and αD	138.7 ± 1.5	142.4 ± 1.4	3.7	9.64 ± 0.17	9.21 ± 0.23	0.43

[a] All statistics are reported as averages for the 20 structures with the lowest NOE violation energies. [b] Medium range NOEs are between residues separated by 2−5 residues, and long-range NOEs are between residues separated by 6 or more residues. [c] Prolines and glycines not included. Analysis with AQUA and Procheck NMR (*47*). [d] Average rmsd calculated for each of the family of 20 structures using a calculated average structure. [e] Non-hydrogens. [f] Includes four helices (residues 223−235, 245−253, 259−269, and 279−293). [g] Calculated with the Interhlx (*58*) program using 20 structures with the lowest NOE violation energies of EH_2 (*9*) and EH_3.

spectra of EH_3 with increasing concentrations of the FW_{PDL} peptide. Titration with FW_{PDL} causes progressive shifts in the ^1H, ^{13}C, and ^{15}N resonances of residues such as Ser^{244} and Trp^{266}, showing that their respective atoms are in fast exchange between the peptide-free and the bound states on the NMR time scale (Figure 2A). Resonances of residues such as Val^{243} and Leu^{253} display line broadening in addition to chemical shift changes; therefore, their respective signals exhibit intermediate exchange. The chemical shift changes were then mapped to the structure of EH_3 (Figure 2B). The most extensive perturbations in backbone amide chemical shifts occur in αB and αC, indicating that these helices are centrally involved in FW peptide binding. Examination of changes in methyl, aromatic, and other side chain chemical shifts in the $^1H/^{13}C$ HSQC spectra narrows the FW-binding site to a pocket formed by residues Leu^{246}, Arg^{249}, Phe^{252}, Leu^{253}, Leu^{262}, Ala^{263}, and Trp^{266} of αB and αC (Figure 2B). Addition of the FW_{MPR} peptide causes perturbations of the amide backbone resonances of a similar set of amino acid residues. However, no line broadening is observed, indicating a faster off-rate for FW_{MPR} than for FW_{PDL}.

The binding site for the NPF peptides was also identified by chemical shift mapping. Addition of NPF_{SYN} causes progressive shifts in ^1H, ^{13}C, and ^{15}N resonances, but in this case no line broadening was observed. The EH_3−NPF interaction is thus exclusively in the fast exchange regime and is likely to be of lower affinity than the EH_3 interaction with the FW_{PDL} peptide. The NMR titration with NPF_{SYN} shows that EH_3 can bind NPF motifs followed by an arginine. This contrasts with a previous study (*3*) reporting negligible affinity between EH_3 and NPF motifs that are not followed by a Leu (NPFL) or a Trp (NPFW). Moreover, the observation of fast exchange for NPF_{SYN} places the affinity of this interaction in the range of other EH−NPF interactions that also display exclusively fast exchange (*9*, *22*).

Mapping the chemical shift changes upon addition of NPF_{SYN} to the structure of EH_3 shows that αB and αC helices exhibit the greatest perturbation of backbone amide resonances, localizing the EH_3−NPF interaction to the same area involved in FW binding (Figure 2C). Analysis of chemical shift perturbations of methyl and aromatic groups shows that the NPF-binding pocket coincides with the FW-binding pocket. In particular, the amino acids Phe^{252}, Leu^{253}, Leu^{262}, and Trp^{266} in EH_3 are involved in both FW and NPF binding (Figure 2B,C). These data are complemented by the observation that NPF binding is inhibited by FW binding and vice versa (*3*). Our data clearly show that there is direct inhibition due to overlapping binding sites and exclude the possibility that an induced conformational change inhibits binding at a second site. The FW- and NPF-binding pocket also corresponds to the NPF-binding sites previously identified in EH_2 (*9*) and mEH_1 (*22*).

Identification of the Calcium-Binding EF-Hand. Calcium occupancy of EF-hands is usually explored by comparing the calcium-bound and free states of a protein. EH_3's requirement for calcium was suggested by its rapid precipita-

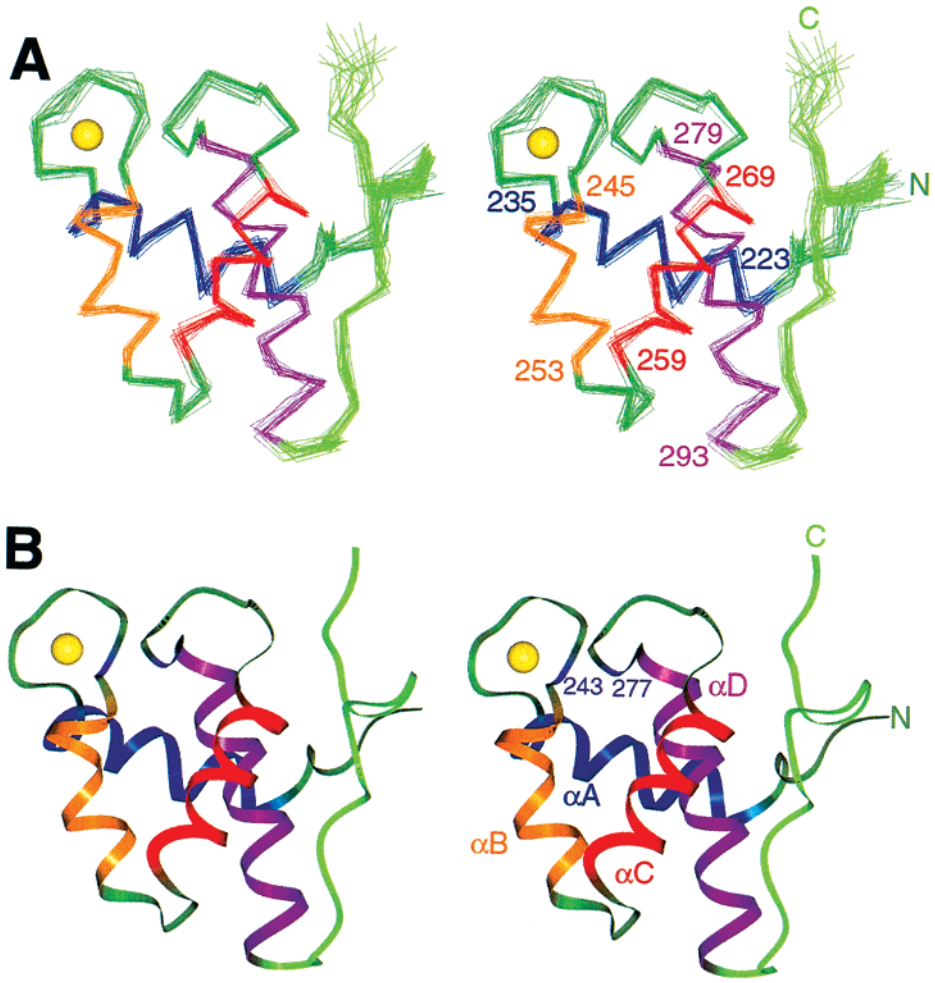

FIGURE 1: Stereo representations of the NMR solution structure of EH_3. The structure of EH_3 consists of two helix−loop−helix motifs. The Cα backbone trace of residues 217−311 is displayed with N and C indicating the N- and C-termini, respectively. αA, in blue, consists of residues 223−235; αB, in orange, consists of residues 245−253; αC, in red, consists of residues 259−269; and αD, in purple, consists of residues 279−293. The position of the calcium ion is depicted as a yellow sphere. Orientation of EH_3 is the same in panels A and B. (A) Superposition of 20 structures with the lowest NOE violation energies. (B) Ribbon diagram of a representative structure. *β*-Sheet contacts occur between Val^{243} and Leu^{277}, which are depicted in blue. All images were created using INSIGHT II (Molecular Simulations Inc.).

tion following the addition of metal chelators. The precipitated protein was denatured and refolded, which required the presence of Ca^{2+} or Mg^{2+}. Figure 3A shows a region of a $^1H/^{15}N$ HSQC spectrum of an EH_3 sample that was refolded in the presence of Mg^{2+} and then titrated with a small amount of Ca^{2+}. Cross-peaks of both the Mg^{2+}-bound and the Ca^{2+}-bound states are present with intensities in an ∼50:50 ratio, indicating that the two states are in similar concentrations and in slow exchange on the NMR time scale. The relatively low calcium concentration (0.38 mM Ca^{2+} vs 160 mM Mg^{2+}) required to generate equivalent amounts of the Ca^{2+}- and Mg^{2+}-bound states shows that EH_3 has a much higher affinity for Ca^{2+} than for Mg^{2+}, analogous to other EF-hand proteins (*51*, *52*). The slow exchange exhibited by EH_3 during the Ca^{2+} titration is indicative of a high affinity for calcium. Therefore, at physiological concentrations of calcium, Ca^{2+} is bound tightly and is required for the structural stability of EH_3.

The presence of a calcium-binding site in only the first helix−loop−helix of EH_3 is evident from chemical shift changes and comparison to other EF-hand loop sequences and structures. The differences between the ^{15}N and ^1H chemical shifts of the Ca^{2+}-bound and Mg^{2+}-bound states of EH_3 show that the first EF-hand loop experiences the greatest perturbation of chemical shifts upon metal replacement (Figure 3B). Magnesium ion ligation typically has the greatest effects on the region in the immediate vicinity of the calcium-binding site of EF-hand proteins (*23*). Thus, the occurrence of the largest chemical shift perturbations in the first helix−loop−helix of EH_3 is consistent with the first EF-hand loop being the only calcium-binding site in EH_3. This is further supported by the presence of a canonical EF-hand sequence (*23*) that contains side chains capable of donating all the oxygen atoms required to coordinate a calcium ion in the first EF-hand loop of EH_3 (Figure 3B). The second helix−loop−helix instead has a Lys at position Y of the canonical calcium-binding sequence that would be expected to repel a divalent cation. Further evidence of a calcium-binding site in only the first EF-hand of EH_3 is based on the side chain conformation of the eighth residue in the first EF-hand loop, the side chain conformation of which correlates with calcium occupancy (*53*). The side chain conformation of Val^{243} in EH_3 is consistent with calcium occupancy exclusively in the first helix−loop−helix. Thus, metal exchange-induced chemical shift changes, EF-hand sequence, and structural arrangements of EH_3 all support the

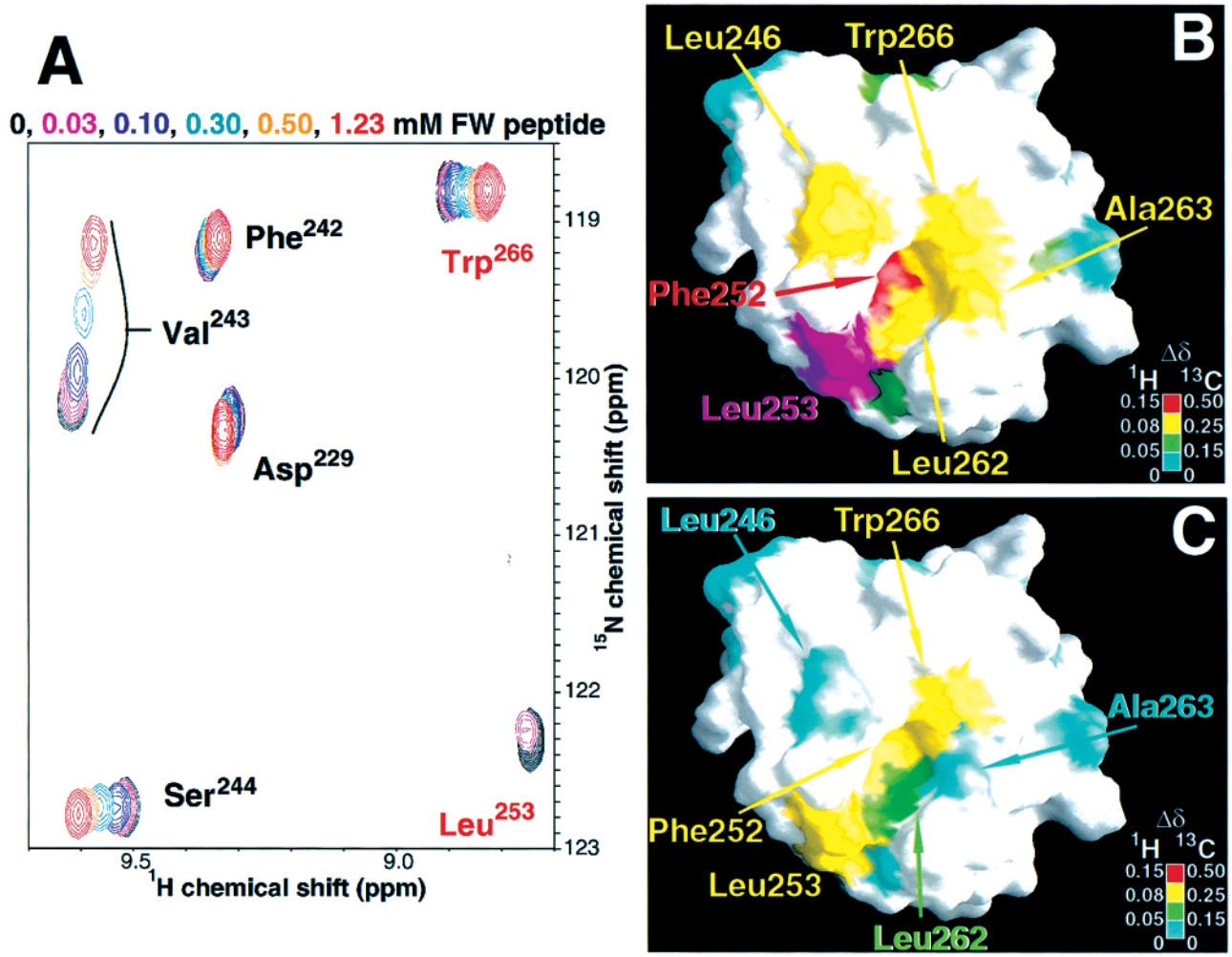

FIGURE 2: FW- and NPF-binding pocket. (A) Selected region of six $^{1}H/^{15}N$ HSQC spectra of EH_3 (0.25 mM) with 0, 0.03, 0.1, 0.3, 0.5, and 1.23 mM DSTPGQVAFW (FW_{PDL}) peptide are superimposed. Colors of the cross-peaks reflect the concentration of the FW_{PDL} peptide as shown above the spectra. Residues in the FW-binding pocket are labeled in red. (B) FW-binding pocket of EH_3. The surface is colored based on the degree of change in ^{1}H and ^{13}C chemical shifts of aromatic, methyl, and other side chain resonances during FW_{PDL} titration; ranges of chemical shift changes are indicated in the inset. Red, yellow, green, and light blue represent large, medium, small, and negligible changes, respectively. Purple indicates residues whose resonances broadened beyond detection. White areas indicate that the difference was not measured. (C) NPF-binding pocket of EH_3. The surface is colored as described in panel B. Images in panels B and C were created using GRASP (*56*).

first EF-hand as being the only calcium-binding EF-hand in EH_3.

Comparisons with Available EH Domain Structures. Despite having only ~39% amino acid identity, EH_3 and EH_2 (*9*) have very similar structures. Superposition of backbone atoms of helical residues in EH_3 and EH_2 results in a rmsd of only 1.1 Å (Figure 4A), and the interhelical distances and angles are similar (Table 1). The main difference in the arrangement of helices is the position of the N-terminal helix; the interhelical angles between αA and αD and between αA and αB are ~12° and ~11° larger, respectively, in EH_3 than in EH_2. The other interhelical angles in EH_3 all differ by less than 4° from their respective positions in EH_2. The overall fold of EH_3 is also shared with mEH_1 (*22*) and the EH domain of POB1 (*54*), although mEH_1 contains additional helical turns in its N- and C-termini, and these regions are also oriented on opposite sides of the domain. At physiological Ca^{2+} concentrations, both EH_3 and EH_2 (*9*) are expected to bind Ca^{2+}, while mEH_1 is not expected to bind Ca^{2+}(*22*). Although Ca^{2+} is required for structural stability of EH_3, its presence or location in the EH domain does not lead to dramatic differences in the overall tertiary structure. Instead, EH domain structure is primarily determined by the conserved residues involved in the packing of the four helices.

Mutagenic and Binding Analysis of EH−FW and EH−NPF Interactions. The binding properties of EH_3 and EH_2 for NPF- and FW-containing peptides were compared using surface plasmon resonance (BIAcore) analysis (Figure 5A,B). All EH−FW and EH−NPF interactions are characterized by fast on- and off-rates that are too fast to be accurately determined by BIAcore. Under these conditions, equilibrium analysis can be used to compare peptide affinities. In agreement with the phage-display study by Paoluzi et al. (*3*), EH_3 displayed affinity for FW_{PDL} and NPF_{RAB}. The affinity of EH_3 for NPF_{RAB} is actually higher than that of EH_2 (Figure 5B), indicating that Rab may be a target of EH_3. This, together with the observation that EH_3 binds NPF_{SYN} with an affinity similar to other EH−NPF interactions (*9*, *22*) as well as FW-containing peptides, suggests that both the NPF and the FW motifs are potential biological targets of EH_3.

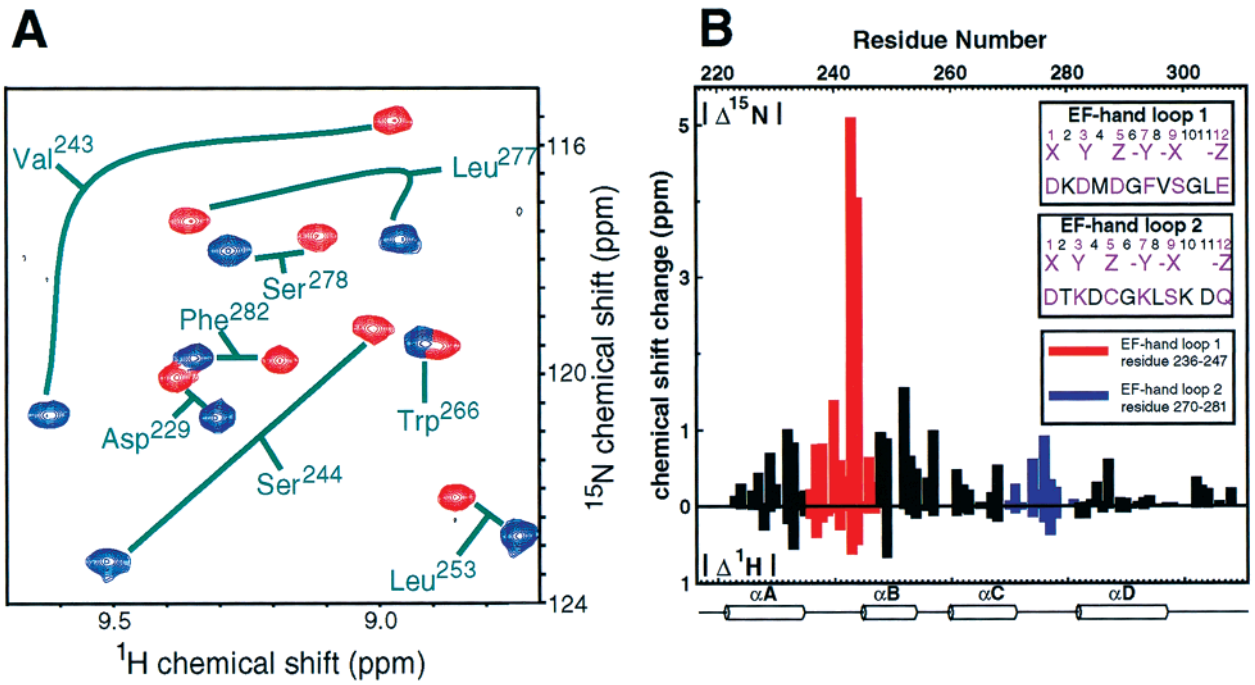

FIGURE 3: Identification of the calcium-binding site in EH_3. (A) Selected region of a $^1H/^{15}N$ HSQC spectrum of EH_3 refolded in the presence of magnesium (160 mM Mg^{2+}) after the addition of 0.55 equiv of calcium (0.38 mM Ca^{2+}). Cross-peaks displayed in blue are from the Ca^{2+}-bound state, and cross-peaks displayed in red are from the Mg^{2+}-bound state. (B) Histogram depicting the absolute value of the change in ^{15}N and ^1H chemical shifts of backbone amide resonances. The absolute value of the change in ^1H chemical shifts ($|\Delta^1H|$) is shown as the bottom of the histogram, and the absolute value of the change in ^{15}N chemical shifts ($|\Delta^{15}N|$) is shown as the top of the histogram. Residues 236−247 compose the first EF-hand loop and are depicted in red. Residues 270−281 compose the second EF-hand loop and are depicted in blue. The secondary structure of EH_3 is shown below the histogram. The amino acid sequence of EF-hand loops 1 and 2 are shown. General EF-hand loop position numbers and letter designations are also shown (*23*, *57*). Residues and numbers in purple correspond to the positions of amino acids potentially involved in the coordination of calcium.

To examine the nature of EH_3's ability to bind both NPF and FW sequences, the binding pocket of EH_3 was compared to the NPF-binding pocket of EH_2. Residues that form the hydrophobic base of the peptide-binding pockets are likely candidates to cause the differences in specificity of EH_3 and EH_2. Phe^{252} in EH_3 and the corresponding Leu^{155} in EH_2 are the only residues that differ in the base of the respective binding pockets (Figure 4B). Phe^{252} is partially exposed in the peptide-free state and borders the conserved tryptophan that is critical for NPF binding (*3*, *9*). It also participates centrally in NPF and FW binding, as evidenced by substantial chemical shift changes. To test whether Phe^{252} enables FW binding, three mutants [EH_3(F252L), EH_3(F252A), and EH_2-(L155F)] were made. The exchange of Phe^{252} to a Leu in EH_3 and the corresponding Leu^{155} to a Phe in EH_2 should decrease or introduce FW affinity of EH_3 or EH_2, respectively. The replacement of Phe^{252} with Leu or Ala in EH_3 reduced but did not abolish FW_{PDL} affinity (Figure 5A). Thus, Phe^{252} contributes to FW recognition. However, replacing Leu^{155} with Phe in EH_2 did not introduce detectable FW affinity, indicating that this residue is not sufficient to establish FW affinity.

The role of Phe^{252} in NPF binding was also explored using the EH_3(F252L) and EH_2(L155F) mutants. The EH_3(F252L) mutant displayed a decrease in NPF_{RAB} affinity relative to wild-type EH_3 (Figure 5B). In contrast, EH_2 and EH_2(L155F) displayed similar affinities for NPF_{RAB}. Thus, this residue is important for EH_3's recognition of NPF_{RAB} but does not alter EH_2's affinity for NPF_{RAB}. Moreover, these mutations indicate that each EH domain possesses binding site residues that make unique contributions to its ligand specificity.

The results of the Phe^{252} and Leu^{155} mutants indicate that mutations of binding site residues can have unique effects on EH domain affinity. Therefore, a mutation that eliminates ligand binding by one EH domain may not alter the binding properties of another EH domain. It has been shown that mutation of Trp^{169} to an Ala in the binding pocket of EH_2 eliminates NPF binding (*3*, *9*). Indeed, the W266A mutation in EH_3 abolished binding to NPF_{RAB}. In addition, this mutation substantially reduced FW_{PDL} affinity, directly implicating Trp^{266} in FW binding (Figure 5A). Furthermore, mutation of Cys^{269} also alters FW affinity (*3*). On the basis of the structure of EH_3, Cys^{269} is positioned underneath the conserved Trp^{266} in the binding pocket (Figure 4C), and its mutation could influence FW affinity by indirectly altering the structure of the binding pocket. Moreover, the position of the conserved Trp differs slightly between the NPF-specific pocket of EH_2 and the FW- and NPF-binding pocket of EH_3 (Figure 4B), implicating the side chain orientation of this residue in EH domain specificity.

Residues that form the sides of the peptide-binding pocket could also influence the specificity of EH domains. The chemical shifts of Leu^{246} and Ala^{263} of EH_3 are more perturbed by FW binding than by NPF binding, suggesting that these residues contact the FW_{PDL} peptide (Figure 2). However, these two residues are not conserved among either NPF- or FW-binding EH domains and are therefore not the primary determinants of FW binding ability. Arg^{249} and Ser^{259} are positioned in the FW- and NPF-binding pocket of EH_3 and differ from the corresponding residues in the NPF-binding pocket of EH_2 (Figure 4C). The position of Ser^{259} is not conserved among either FW- or NPF-binding EH

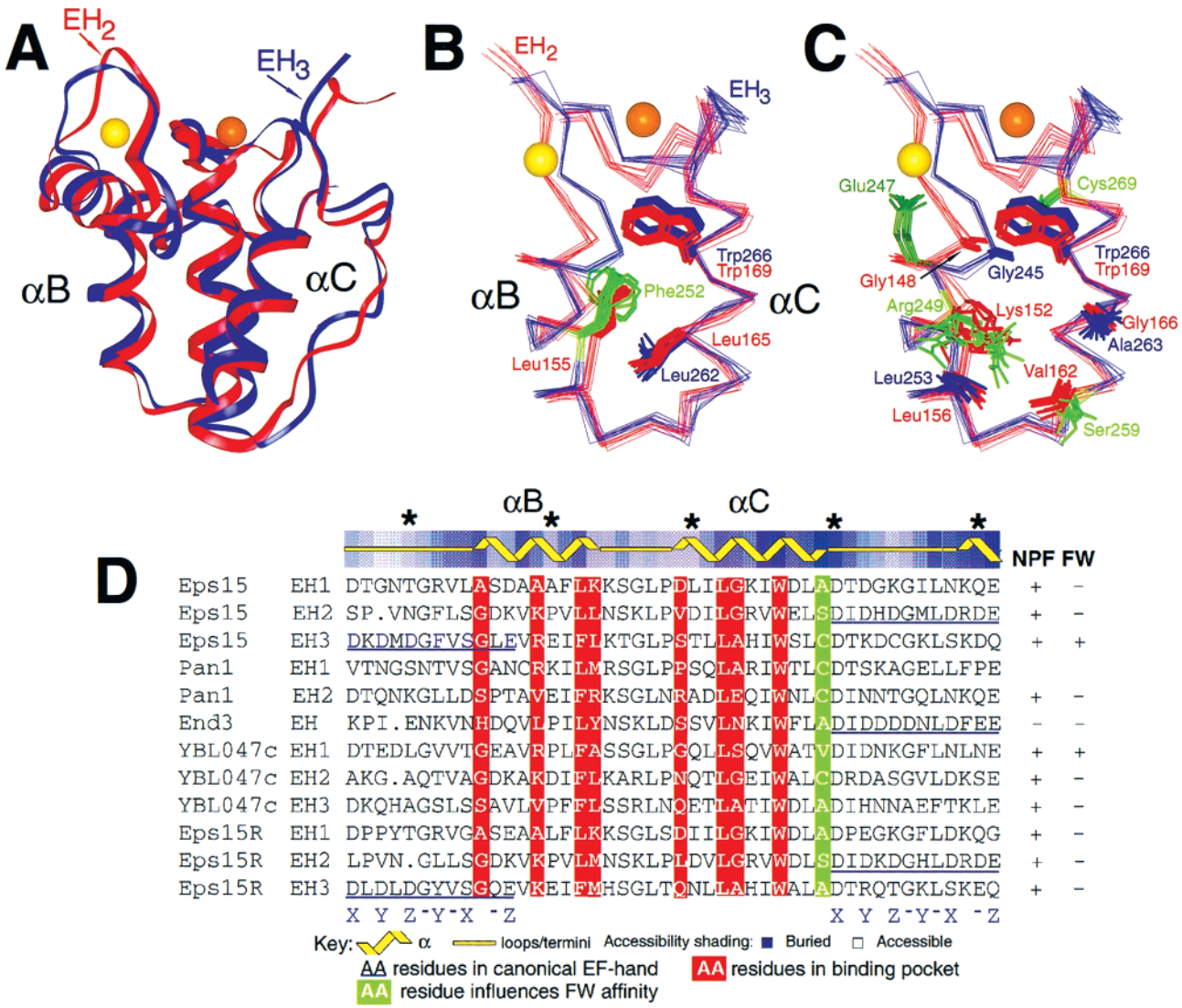

FIGURE 4: Comparison of the binding pockets of EH_3, EH_2, and other EH domains. (A) Helices αA, αB, αC, and αD of EH_3 and EH_2 were superimposed. EH_3 is in blue, and the position of its coordinated calcium is depicted as a yellow sphere. EH_2 is in red, and the position of its coordinated calcium is depicted as an orange sphere. The orientation of the EH domains are similar to that in Figure 1. (B) Backbone atoms of helices αB and αC of the 10 lowest NOE energy structures of EH_3 and EH_2 are superimposed. EH_3 (αB and αC) and its calcium are in blue and yellow, respectively. EH_2 (αB and αC) and its calcium are in red and orange, respectively. EH_3 residues with heavy atoms depicted in green are candidates for contributing to FW specificity. The core residues of the binding pockets are shown. (C) Residues that line the binding pocket are depicted. The view and coloring are as in panel B. (D) Amino acid sequence alignment of the two EF-hand loops and the second and third helices of selected EH domains. The secondary structure of EH_3, generated with Procheck NMR (*47*), is shown above the sequences, and every 10th residue is marked with an asterisk (*), with the leftmost one indicating residue 240 of EH_3. The peptide motif selected by each EH domain (*3*) is indicated by a "+" or "−". The coloring of the key amino acids is indicated in the figure. Images in panels A−C were created using INSIGHT II (Molecular Simulations Inc.).

domains, making it an unlikely determinant of FW binding. In contrast, all EH domains that do not select for FW-containing peptides do not possess an arginine at the position corresponding to residue 249 of EH_3 (*3*) (Figure 4D). Also, the ^1H and ^{15}N resonances of Arg^{249} exhibit large chemical shift changes during FW_{PDL} titration, indicating that this residue is likely in contact with an aromatic ring of FW_{PDL}. Thus, of these residues, Arg^{249} is most likely to contribute to EH_3's FW affinity.

The contribution of Arg^{249} to FW affinity was tested with three mutants, EH_3(R249K), EH_3(R249A), and EH_2(K152R). The EH_3(R249A) mutant resulted in a substantial decrease in EH_3's FW_{PDL} affinity (Figure 5C). Thus, Arg^{249} is important for FW specificity. Dramatic decreases in EH_3's FW_{PDL} affinity were also observed with the EH_3(R249K) mutant. Therefore, even a conservative change at this position is detrimental to FW binding. However, the EH_2(K152R) mutant did not introduce FW-binding ability to EH_2. These results imply that Arg^{249} is partially responsible for FW recognition, but this residue, like Phe^{252}, is not sufficient to introduce FW affinity.

Arg^{249} is also partially responsible for NPF recognition by EH_3. EH_2(K152R) and wild-type EH_2 displayed similar affinities for NPF_{RAB}, while the EH_2(K152A) mutant displayed a moderate decrease in NPF_{RAB} affinity (Figure 5D). In contrast, the EH_3(R249K) and EH_3(R249A) mutants displayed much more dramatic decreases in NPF_{RAB} affinity (Figure 5D), showing the importance of Arg^{249} in NPF_{RAB} recognition by EH_3. Moreover, the disparate affects of these mutations on EH domain ligand affinities further validates the existence of unique specificity determinants in individual EH domains.

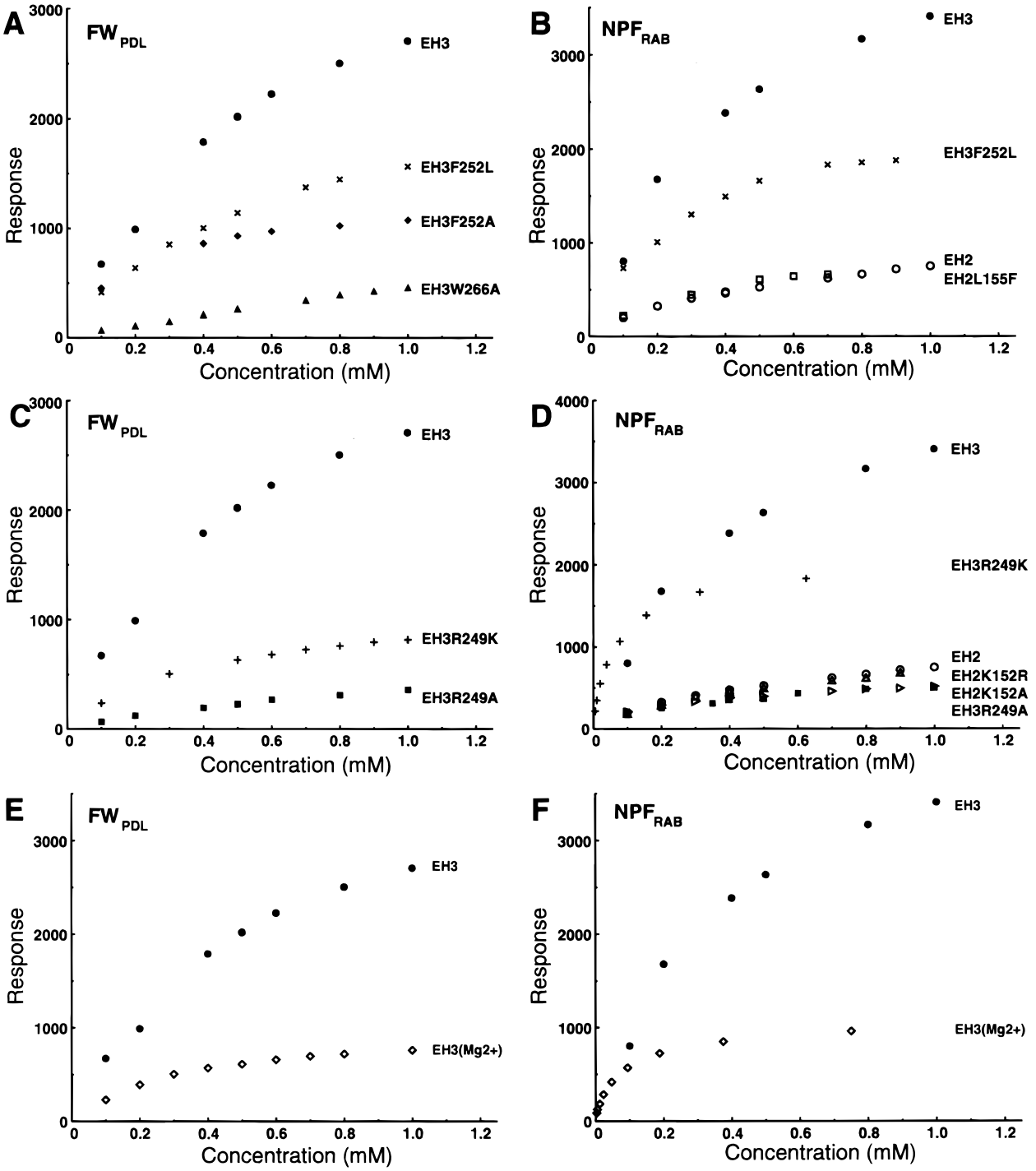

FIGURE 5: Relative binding affinities of EH domains. The BIAcore equilibrium binding response values for different concentrations of protein for the binding of either FW_{PDL} or NPF_{RAB} are shown. The peptide immobilized on the chip for panels A, C, and E is FW_{PDL} and for panels B, D, and F is NPF_{RAB}. The symbols are as follows: (●) EH_3, (×) EH_3F252L, (◆) EH_3F252A, (▲) EH_3W266A, (+) EH_3R249K, (■) EH_3R249A, (○) EH_2, (□) EH_2L155F, (△) EH_2K152R, and (open triangle right) EH_2K152A. Magnesium-bound EH_3 [$EH_3(Mg^{2+})$] is represented by (◇). Interactions of EH_2 and all mutants of EH_2 with the FW_{PDL} peptide were too weak to be detected.

Finally, the position of the calcium-binding sites in EH domains might contribute to ligand-binding affinities. The coordination of calcium in the first EF-hand of EH_3 affects the shape of the FW- and NPF-binding pocket relative to that of EH_2. The superposition of EH_3 and EH_2 shows that Gly^{245} is ~2 Å from the position of Gly^{148}, the corresponding residue in EH_2 (Figure 4C). This difference in the structures is presumably caused by the coordination of calcium by Glu^{247} and other residues in the first EF-hand of EH_3. Calcium coordination also results in a difference of 3.5° in the angle between the two peptide binding helices of EH_3 and EH_2 (Table 1) and a narrower binding pocket (Figure 4C). Ligation of a smaller Mg^{2+} ion by an EF-hand requires reorganization of the oxygen-donating residues due to magnesium's strong preference for 6-fold coordination (*23*). The ligation is generally accomplished through the switching of the conserved bidentate ligand, Glu^{247} in EH_3, to a monodentate ligand (*23*). However, more complex reorganizations have been observed in other EF-hands in which several of the oxygens donated by residues in the EF-hand

loop are replaced with coordinating waters (*52*). The latter type of reorganization is also associated with larger perturbations in the packing of the helices. Magnesium ligation by EH_3 resulted in surprisingly large decreases in FW- and NPF-binding affinities (Figure 5E,F). Thus, the conformational change induced by Mg^{2+} ligation influences the peptide-binding properties of EH_3, and the binding pocket shape as dictated by calcium ligation contributes to EH_3's ligand affinity. Furthermore, since the presence and position of calcium-binding sites vary throughout the EH domain family, calcium ligation could represent an evolutionary mechanism to fine-tune EH domain specificity.

Structural and mutational analysis of EH domains has provided important new insights into the molecular mechanisms of EH−FW and EH−NPF interactions. EH_3 has been shown to bind FW and NPF ligands with affinities typical of other EH−NPF interactions, implicating both NPF and FW sequences as potential biological targets of EH_3. Further support for a biological role of the EH−FW interaction is the demonstration that EH_3 binds to a peptide mimicking the FW-internalization motif of MPR. The presence of Eps15 in clathrin-uncoated vesicles, including endosomes (*55*) where EH_3 could interact with MPR, warrants further investigation into a possible Eps15−MPR interaction.

NMR analysis unequivocally shows that FW and NPF bind in the same pocket, and mutational analysis has implicated the same residues in binding each peptide. Specifically, Phe^{252}, Trp^{266}, and Arg^{249} have been directly implicated in FW recognition. However, none of these residues completely abolished the EH_3−FW interaction, and introduction of these residues alone in EH_2 is unable to induce FW-binding ability. In addition, the coordination of calcium in the first EF-hand loop, which establishes the shape of the peptide-binding pocket, also contributes to FW recognition. Together, these results indicate that FW recognition cannot be attributed to a single residue but that multiple binding site residues along with the influences of calcium-ligation act in concert in defining EH_3 specificity. Moreover, mutation of binding site residues such as Phe^{252} and Arg^{249}, which substantially affect EH_3 ligand binding, or of the corresponding Leu^{155} and Lys^{152} residues, which leave EH_2's binding properties intact, attests to the uniqueness of ligand recognition by EH domains. As a consequence, multiple factors need to be considered for the a priori identification of NPF or FW specificity determinants. Further analysis of EH domains that contain multiple mutations and NMR structures of EH−NPF and EH−FW complexes will also aid in our understanding of the underlying mechanisms of EH domain ligand recognition.

ACKNOWLEDGMENT

We thank R. E. Carter for guidance in cloning and mutagenesis, J. Mamay for computational support, A. Sorkin for Eps15 cDNA and discussions, R. Muhandiram and L. E. Kay for NMR pulse sequences, J. Thompson of the Department of Pharmacology DNA sequencing facility of the University of Colorado Health Sciences Center, and S. Famigliette for assistance with the BIAcore.

REFERENCES

1. Santolini, E., Salcini, A. E., Kay, B. K., Yamabhai, M., and Di Fiore, P. P. (1999) *Exp. Cell Res. 253*, 186−209.
2. Salcini, A. E., Confalonieri, S., Doria, M., Santolini, E., Minenkova, O., Pelicci, P. G., and Di Fiore, P. P. (1997) *Genes Dev. 11*, 2239−2249.
3. Paoluzi, S., Castagnoli, L., Lauro, I., Salcini, A. E., Coda, L., Fre, S., Confalonieri, S., Pelicci, P. G., Di Fiore, P. P., and Cesareni, G. (1998) *EMBO J. 17*, 6541−6550.
4. Kohtz, D. S., and Puszkin, S. (1998) *J. Biol. Chem. 263*, 2144−2155.
5. Haffner, C., Takei, K., Chen, H., Ringstad, N., Hudson, A., Butler, M. H., Salcini, A. E., Di Fiore, P. P., and De Camilli, P. (1997) *FEBS Lett. 419*, 175−180.
6. Chen, H., Fre, S., Slepnev, V. I., Capua, M. R., Takei, K., Butler, M. H., Di Fiore, P. P., and De Camilli, P. (1998) *Nature 394*, 793−797.
7. Schweizer, A., Kornfeld, S., and Rohrer, J. (1997) *Proc. Natl. Acad. Sci. U.S.A. 94*, 14471−14476.
8. Johnson, K., Chan, W., and Kornfeld, S. (1990) *Proc. Natl. Acad. Sci. U.S.A. 87*, 10010−10014.
9. de Beer, T., Carter, R. E., Lobel-Rice, K. E., Sorkin, A., and Overduin, M. (1998) *Science 281*, 1357−1360.
10. Di Fiore, P. P., Pelicconi, P. G., and Sorkin, A. (1997) *Trends Biochem. Sci. 22*, 411−413.
11. Tebar, F., Confalonieri, S., Carter, R. E., Di Fiore, P. P., and Sorkin, A. (1997) *J. Biol. Chem. 272*, 15413−15418.
12. Wong, W. T., Schumacher, C., Salcini, A. E., Romano, A., Castagnino, P., Pelicci, P. G., and Di Fiore, P. P. (1995) *Proc. Natl. Acad. Sci. U.S.A. 92*, 9530−9534.
13. Yamabhai, M., Hoffman, N. G., Hardison, N. L., McPherson, P. S., Castagnoli, L., Cesareni, G., and Kay, B. K. (1998) *J. Biol. Chem. 273*, 21401−31407.
14. Page, L. J., Sowerby, P. J., Lui, W. W. Y., and Robinson, M. S. (1999) *J. Cell Biol. 146*, 993−1004.
15. Mintz, L., Galperin, E., Pasmanik-Chor, M., Tulzinsky, S., Bromberg, Y., Kozak, C. A., Joyner, A., Fein, A., and Horowitz, M. (1999) *Genomics 59*, 66−76.
16. Benmerah, A., Gagnon, J., Bègue, B., Mégarbané, B., Dautry-Varsat, A., and Cerf-Bensussan, N. (1995) *J. Cell Biol. 131*, 1831−1838.
17. Benmerah, A., Bègue, B., Dautry-Varsat, A., and Cerf-Bensussan, N. (1996) *J. Biol. Chem. 271*, 12111−12116.
18. van Delft, S., Schumacher, C., Hage, W., Verkleij, A. J., and van Bergen en Henegouwen, P. M. P. (1997) *J. Cell Biol. 136*, 811−821.
19. Iannolo, G., Salcini, A. E., Gaidarov, I., Goodman, O. B., Jr., Baulida, J., Carpenter, G., Pelicci, P. G., Di Fiore, P. P., and Keen, J. H. (1997) *Cancer Res. 57*, 240−245.
20. Sengar, A. S., Wang, W., Bishay, J., Cohen, S., and Egan, S. E. (1999) *EMBO J. 18*, 1159−1171.
21. Coda, L., Salcini, A. E., Confalonieri, S., Pelicci, G., Sorkina, T., Sorkin, A., Pelicci, P. G., and Di Fiore, P. P. (1998) *J. Biol. Chem. 273*, 3003−3012.
22. Whitehead, B., Tessari, M., Carotenuto, A., van Bergen en Henegouwen, P. M. P., and Vuister, G. W. (1999) *Biochemistry 38*, 11271−11277.
23. Strynadka, N. C. J., and James, M. N. G. (1989) *Annu. Rev. Biochem. 58*, 951−98.
24. Fin, B. E., Evenäs, J., Drakenberg, T., Waltho, J. P., Thulin, E., and Forsén, S. (1995) *Nat. Struct. Biol. 2*, 777−783.
25. Strynadka, N. C. J., Cherney, M., Sielecki, A. R., Li, M. X., Smillie, L. B., and James, M. N. G. (1997) *J. Mol. Biol. 273*, 238−255.
26. Skelton, N. J., Kordel. J., and Chazin, W. J. (1995) *J. Mol. Biol. 249*, 441−462.
27. Altieri, A. S., Hinton, D. P., and Byrd, R. A. (1995) *J. Am. Chem. Soc. 117*, 7566−7567.
28. Delaglio, F., Grzesiek, S., Vuister, G. W., Zhu, G., Pfiefer, J., and Bax, A. (1995) *J. Biomol. NMR 6*, 277−293.
29. Garret, D. S., Powers, R., Gronenborn, A. M., and Clore, G. M. (1991) *J. Magn. Reson. 95*, 214−220.
30. Enmon, J. L., de Beer, T., and Overduin, M. (2000) *J. Biomol. NMR 16*, 81−82.
31. Grzesiek, S., Anglister, J., and Bax, A. (1993) *J. Magn. Reson. B 101*, 114−119.

32. Kay, L. E., Xu, G. Y., Singer, A. U., Muhandiram, D. R., and Forman-Kay, J. D. (1993) *J. Magn. Reson. B 101*, 333−337.
33. Muhandiram, D. R., and Kay, L. E. (1994) *J. Magn. Reson. B 103*, 203−216.
34. Yamazaki, T., Forman-Kay, J. D., and Kay, L. E. (1993) *J. Am. Chem. Soc. 115*, 11054−11055.
35. Vuister, G. W., and Bax, A. (1993) *J. Am. Chem. Soc. 115*, 7772−7777.
36. Kay, L. E., and Bax, A. (1990) *J. Magn. Reson. 86*, 110−126.
37. Wishart, D. S., and Sykes, B. D. (1994) *J. Biomol. NMR 4*, 171−180.
38. Marion, D., Driscoll, P. C., Kay, L. E., Windfield, P. T., Bax, A., Gronenborn, A. M., and Clore, G. M. (1989) *Biochemistry 28*, 6150−6156.
39. Fesik, S. W., and Zuiderweg, E. R. P. (1988) *J. Magn. Reson. 78*, 588−593.
40. Vuister, G. W., Clore, M. G., Gronenborn, A. M., Powers, R., Garret, D. S., Tschudin, R., and Bax, A. (1993) *J. Magn. Reson. B 101*, 210−213.
41. Pascal, S. M., Muhandiram, T., Yamazaki, T., Forman-Kay, J. D., and Kay, L. E. (1994) *J. Magn. Reson. B 103*, 197−201.
42. Fletcher, C. M., Jones, D. N. M. Diamond, R., and Neuhaus, D. (1996) *J. Biomol. NMR 8*, 292−310.
43. Chattopadhyaya, R., Meador, W. E., Means, A. R., and Quiocho, F. A. (1992) *J. Mol. Biol. 228*, 1177−1192.
44. Declercq, J. P., Tinant, B., Parello, J., and Rambaud, J. (1991) *J. Mol. Biol. 220*, 1017−1039.
45. Svensson, L. A., Thulin, E., and Forsén, S. (1992) *J. Mol. Biol.* 223, 601−606.
46. Brunger, A. T. (1992) *X-PLOR*, Version 3.1, A System for X-ray Crystallography and NMR, Yale University Press, New Haven, CT.
47. Laskowski, R. A., Rullman, J. A. C., MacArthur, R., Kaptein, J. M., and Thorton, J. (1996) *J. Biomol. NMR 8*, 477−486.
48. Frenkiel, T., Bauer, C., Carr, M. D., Birdsall, B., and Freeney, J. (1990) *J. Magn. Reson. 93*, 420−425.
49. Bodenhausen, G., and Ruben, D. J. (1980) *Chem. Phys. Lett. 69*, 185−189.
50. Kay, L. E., Keifer, P., and Saarinen, T. (1992) *J. Am. Chem. Soc. 114*, 10663−10665.
51. Drake, S. K., Lee, K. L., and Falke, J. L. (1996) *Biochemistry 35*, 6697−6705.
52. Andersson, M., Malmendal, A., Linse, S., Ivarsson, I., Forsén, S., and Svensson, L. A. (1997) *Protein Sci. 6*, 1139−1147.
53. Biekofsky, R. R., Martin, S. R., Browne, J. P., Bayley, P. M., and Feeney, J. (1998) *Biochemistry 37*, 7617−7629.
54. Koshiba, S., Kigawa, T., Iwahara, J., Kikuchi, A., and Yokoyama S. (1999) *FEBS Lett. 442*, 138−142.
55. Torrisi, M. R., Lotti, L. V., Belleudi, F., Gradini, R., Salcini, A. E., Confalonieri, S., Pelicci, P. G., and Di Fiore, P. P. (1999) *Mol. Biol. Cell 10*, 417−434.
56. Nicholls, A., Sharp, K. A., and Honig, B. (1991) *Proteins 11*, 281−296.
57. Kretsinger, R. H. (1980) *CRC Crit. Rev. Biochem. 8*, 119−174.
58. Nico Tjandra. Interhlx program (October 20, 1998) http://diana.oci.utoronto.ca/ikura/datasoft.html.

BI9927383